PNAS RESEARCH ARTICLE | EARTH, ATMOSPHERIC, AND PLANETARY SCIENCES OPEN ACCESS

Rapid timescale for an oxic transition during the Great Oxidation Event and the instability of low atmospheric O_2

Nicholas F. Wogan[a,b,1], David C. Catling[a,b], Kevin J. Zahnle[c], and Mark W. Claire[b,d,e]

Edited by Mark Thiemens, University of California San Diego, La Jolla, CA; received March 30, 2022; accepted August 8, 2022

The Great Oxidation Event (GOE), arguably the most important event to occur on Earth since the origin of life, marks the time when an oxygen-rich atmosphere first appeared. However, it is not known whether the change was abrupt and permanent or fitful and drawn out over tens or hundreds of millions of years. Here, we developed a one-dimensional time-dependent photochemical model to resolve time-dependent behavior of the chemically unstable transitional atmosphere as it responded to changes in biogenic forcing. When forced with step-wise changes in biogenic fluxes, transitions between anoxic and oxic atmospheres take between only 10^2 and 10^5 y. Results also suggest that O_2 between $\sim 10^{-8}$ and $\sim 10^{-4}$ mixing ratio is unstable to plausible atmospheric perturbations. For example, when atmospheres with these O_2 concentrations experience fractional variations in the surface CH_4 flux comparable to those caused by modern Milankovich cycling, oxygen fluctuates between anoxic ($\sim 10^{-8}$) and oxic ($\sim 10^{-4}$) mixing ratios. Overall, our simulations are consistent with possible geologic evidence of unstable atmospheric O_2, after initial oxygenation, which could occasionally collapse from changes in biospheric or volcanic fluxes. Additionally, modeling favors mid-Proterozoic O_2 exceeding 10^{-4} to 10^{-3} mixing ratio; otherwise, O_2 would periodically fall below 10^{-7} mixing ratio, which would be inconsistent with post-GOE absence of sulfur isotope mass-independent fractionation.

Great Oxidation Event | photochemistry | oxygen

Significance

Understanding the rise of atmospheric oxygen on Earth is important for assessing precursors to complex life and for evaluating potential future detections of oxygen on exoplanets as signs of extraterrestrial biospheres. However, it is unclear whether Earth's initial rise of O_2 was monotonic or oscillatory, and geologic evidence poorly constrains O_2 afterward, during the mid-Proterozoic (1.8 billion to 0.8 billion years ago). Here, we used a time-dependent photochemical model to simulate oxygen's rise and the stability of subsequent O_2 levels to perturbations in supply and loss. Results show that large oxygen fluctuations are possible during the initial rise of O_2 and that Mesoproterozoic O_2 had to exceed 0.01% volume concentration for atmospheric stability.

Abundant atmospheric O_2 at 21% by volume is the most distinctive and consequential feature of Earth's atmosphere. Produced by cyanobacteria, algae, and plants, O_2 is a clear sign of our biosphere that is detectable across interstellar space by telescopic spectroscopy (1). Oxygen permits aerobic respiration, the only known metabolism with sufficient energy yield to sustain complex animal life (2). However, for about the first half of Earth's 4.5-billion-year-old history, the atmosphere had negligible O_2 (e.g., ref. 3). This changed ~2.4 billion years ago.

The timing of the Great Oxidation Event (GOE) and the magnitude of atmospheric O_2 concentrations before and after the GOE can be constrained by the geologic record of sulfur isotopes in combination with photochemical models. Archean and earliest Proterozoic sedimentary minerals contain sulfur isotopes with characteristic mass-independent fractionation (MIF) which abruptly disappears 2.4 billion years ago (4). Sulfur MIF in marine sediments likely requires that atmospheric photochemistry produce elemental sulfur, S_8 (for explanation, see the introduction in ref. 5) (6, 7). Zahnle et al. (5) used a one-dimensional (1D) photochemical model to show that atmospheric S_8 production only occurs when atmospheric O_2 is below $\sim 2 \times 10^{-7}$ mixing ratio. An often cited threshold of 2×10^{-6} was from an earlier photochemical model that did not simulate atmospheres with surface O_2 mixing ratios between 2×10^{-6} and $\sim 10^{-15}$ (6). Therefore, the disappearance of the sulfur isotope MIF signal at 2.4 Ga is strong evidence that O_2 first rose above 2×10^{-7} mixing ratio then.

Geologic evidence may suggest that the GOE was not a single monotonic rise of oxygen but characterized by oscillations. Using U-Pb dating, Gumsley et al. (8) updated the chronology of sulfur isotope MIF in the stratigraphic record, finding evidence for two oxic-to-anoxic transitions between ~2.4 and ~2.3 Ga. More recently, Poulton et al. (9) report 2.3 Ga to 2.2 Ga marine sediments with sulfur isotopes consistent with approximately five oxic-to-anoxic transitions. Fluctuating O_2 levels coincide with three to four widespread glaciations, indicating extreme climate instability (10). Overall, geochemical evidence tentatively suggests that O_2 concentrations and climate were unstable for 200 million years until 2.2 Ga, which marks the most recent estimated timing of the permanent oxygenation of the atmosphere (9). However, interpretations of oscillating O_2 have been questioned (11). While the geologic evidence for the O_2 oscillations remains equivocal, the data have raised significant questions regarding the feasibility and timescales for Earth's great oxidation. Some have argued that the oxygen-rich

Author contributions: N.F.W., D.C.C., and K.J.Z. designed research; N.F.W. performed research; N.F.W., D.C.C., K.J.Z., and M.W.C. analyzed data; N.F.W. and D.C.C. wrote the paper; and N.F.W. and K.J.Z. developed the modeling code.

The authors declare no competing interest.

This article is a PNAS Direct Submission.

[1]To whom correspondence may be addressed. Email: wogan@uw.edu.

This article contains supporting information online at https://www.pnas.org/lookup/suppl/doi:10.1073/pnas.2205618119/-/DCSupplemental.

Published September 6, 2022.

atmosphere is more stable than an oxygen-poor atmosphere (12), which favors a single rise of O_2 instead of O_2 oscillations.

Evidence for O_2 instability and the time-dependent behavior of O_2 concentrations has not been reconciled with atmospheric photochemical models. All previous models treated the GOE as successive photochemical steady states (5, 6, 13–19). A photochemical steady state occurs when no atmospheric species changes concentration over time, because their production and loss from reactions and surface sources (e.g., volcanoes or biology) are balanced. Such steady-state calculations have been crucial for understanding the GOE by contextualizing sulfur isotope MIF observations (5, 6), and establishing the relationship between atmospheric O_2 concentrations and the degree to which O_3 blocks UV photons from Earth's surface (i.e., O_3 shielding) (13, 15, 16), but they do not evaluate time-dependent changes and transient imbalances, or characteristic timescales.

Several theories for the rise of O_2 suggest that it relied on a global redox titration over 10^8 y to 10^9 y involving oxidation of the upper mantle and/or crust, plausibly driven by hydrogen escape, which led to a tipping point where the source flux of O_2 exceeded a kinetically rapid O_2 sink from volcanic and metamorphic reductants (20–24). Beyond the tipping point, O_2 flooded the atmosphere, reaching a new, long-term balance limited by oxidative weathering.

Here, we developed a time-dependent 1D photochemical model capable of investigating changes of O_2 at the tipping point itself over timescales of 10^2 y to 10^5 y rather than the longer-term planetary changes which initiated the GOE. We simulate changing O_2 as a time-dependent evolution, in contrast to the steady-state approach used in previous studies (e.g., ref. 13), because O_2 can change on relatively rapid timescales that are not well characterized by steady states. With our model, we compute the time required for an anoxic-to-oxic atmospheric transition, and the time required for deoxygenation. Additionally, we investigate the stability of O_2 concentrations against perturbations to surface gas fluxes produced by biology. Finally, we use our model results to better constrain O_2 levels and stability during the GOE (starting at ~2.4 Ga), and during the mid-Proterozoic eon (1.8 Ga to 0.8 Ga).

Results

To investigate the time-dependent behavior of O_2 during the GOE, we first computed grids of photochemical steady-state atmospheres. These steady states establish the context for time-dependent photochemical modeling described in subsequent sections. Fig. 1 shows the predicted steady-state surface O_2 mixing ratio (Fig. 1*A*), the surface CH_4 mixing ratio (Fig. 1*B*), and the precipitation of atmospheric S_8 (gray shading) as a function of surface O_2 flux between 3×10^9 and 10^{13} molecules per $cm^2 \cdot s^{-1}$, and CH_4 flux/O_2 flux ratios between 0.27 and 0.49 where gas fluxes are those entering the atmosphere. The surface O_2 fluxes reported here are net emissions into the atmosphere which exclude recycling within the biosphere. For reference, a comparable model of the modern Earth requires a surface O_2 flux of 10^{12} molecules per $cm^2 \cdot s^{-1}$, and a CH_4 flux/O_2 flux of 0.09 (CH_4 flux = $\sim 9 \times 10^{10}$ molecules per $cm^2 \cdot s^{-1}$) (16). We consider a CH_4 flux/O_2 flux ratio close to 0.5 to be more realistic for the Late Archean, prior to the GOE, because this ratio is expected if oxygenic photosynthesis is balanced by methanogenesis. In net (21), where "CH_2O" represents organic matter,

$$\begin{aligned} CO_2 + H_2O &\rightarrow CH_2O + O_2 && \text{(Oxygenic Photosynthesis)} \\ 2CH_2O &\rightarrow CH_4 + CO_2 && \text{(Methanogenesis)} \\ CO_2 + 2H_2O &\rightarrow CH_4 + 2O_2 && \text{(Net).} \end{aligned} \quad [1]$$

The CH_4 flux/O_2 flux ratio is smaller than 0.5 on modern Earth largely because of the microbial anerobic oxidation of methane via SO_4^{2-} in ocean sediments, a process that was unimportant in the anoxic mid-Archean ocean with little sulfate (25–27). We include O_2 fluxes several orders of magnitude smaller than the modern value ($\sim 10^{12}$ molecules per $cm^2 \cdot s^{-1}$) because of evidence for smaller primary productivity during the Proterozoic eon (28, 29).

Recall that atmospheric S_8 deposition is considered necessary to preserve sulfur isotope MIF in ocean sediments (6). We find that S_8 production is not possible above a $\sim 10^{-7}$ O_2 mixing ratio (the gray-to-white shading boundary in Fig. 1), consistent with previous results (5).

Fig. 1 uses Archean outgassing surface fluxes for CO, H_2, H_2S, and SO_2 listed in Table 1, with the CO_2 surface mixing ratio fixed to 1% for all model runs—a reasonable value for the Late Archean according to carbon cycle modeling (30). Additionally, over the same span of surface O_2 fluxes and H_2 flux/O_2 flux ratios, we compute photochemical steady states for the modern fluxes for CO, CH_4, H_2S, and SO_2 listed in Table 1, again fixing CO_2 to 1%. The results are shown in *SI Appendix*, Fig. S1.

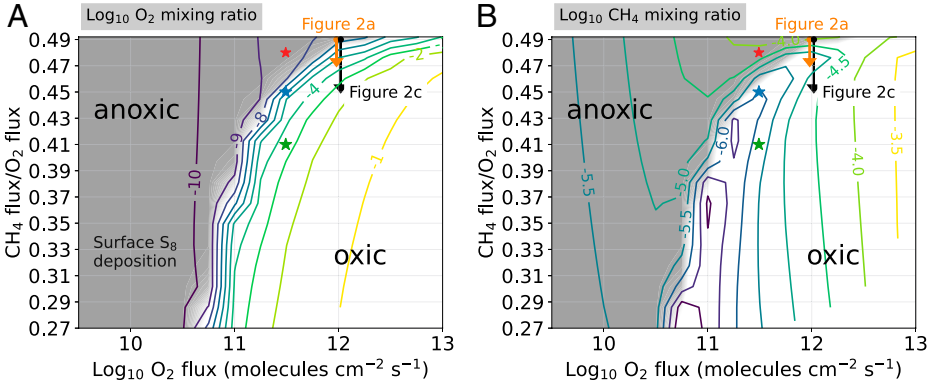

Fig. 1. Colored contours show photochemical steady states of (*A*) $\log_{10}$ surface O_2 mixing ratio and (*B*) $\log_{10}$ surface CH_4 mixing ratio as a function of $\log_{10}$ O_2 surface flux and CH_4 flux/O_2 flux. Gray shading indicates the magnitude of elemental S_8 production in the atmosphere, which is considered essential for the preservation of sulfur isotope MIF in marine sediments. Peak S_8 production is $\sim 10^7$ molecules per $cm^2 \cdot s^{-1}$. Gray shading fades to white for S_8 production less than 10^{-10} molecules per $cm^2 \cdot s^{-1}$, a negligibly small value. Arrows labeled "Figure 2a" and "Figure 2c" indicate start and end points for time-dependent photochemical models of the oxic transition shown in Fig. 2 *A* and *C*. Red, blue, and green stars are the initial conditions used in the simulations shown in Fig. 4 *B*, *C*, and *D*, respectively.

Table 1. Fixed surface flux boundary conditions for SO_2, H_2S, H_2, and CO used in this study

Model	SO_2	H_2S	H_2	CO
Archean outgassing*	10^{10}	10^{9}	3×10^{10}	3×10^{9}
Modern values†	3.5×10^{9}	3.5×10^{8}	1.22×10^{8}	2.65×10^{11}

All fluxes have units of molecules per square centimeter per second.
*The same fluxes as the "Archean High" values from table 1 in Zahnle et al. (5).
†Surface flux values required to reproduce the concentration of each gas in modern Earth's atmosphere. These values are also the "Case 1" fluxes described in Gregory et al. (16).

In the following sections, we calculate the time required to transition between different steady-state atmospheres shown in Fig. 1 and *SI Appendix*, Fig. S1.

The Timescale of Atmospheric Oxygenation. The orange arrow labeled "Figure 2a" in Fig. 1 corresponds to the approximate start and end states of the time-dependent photochemical model run shown in Fig. 2*A*. The model starts with an atmosphere at a steady state, then, at $t = 0$ y, we impose a stepwise decrease in the surface methane flux from 4.9×10^{11} to 4.7×10^{11} molecules per $cm^2 \cdot s^{-1}$ (we keep the surface O_2 flux constant at 10^{12} molecules per $cm^2 \cdot s^{-1}$). This perturbation causes O_2 to rise from 3×10^{-8} to 3×10^{-5} mixing ratio over 3,500 y, eliminating photochemical S_8 production.

The O_2 transition in Fig. 2 *A*, *i* is modulated by O_3 shielding of tropospheric H_2O (13). When a stratospheric O_3 layer begins to develop, OH production from H_2O decreases (Fig. 2 *A*, *ii*). Decreasing OH concentrations prevent the mutual annihilation of O_2 and CH_4 (by $CH_4 + OH \rightarrow CH_3 + H_2O$ followed by $CH_3 + O_2 \rightarrow$ products), so O_2 levels increase. The mixing ratio of CH_4 also rebounds. O_3 shielding (protecting life on the surface from harmful solar UV radiation) is just barely beginning to operate in this example compared to modern Earth. After the atmosphere reaches a new steady state, the atmospheric column has 3×10^{17} O_3 molecules per cm^2, some 26 times smaller than the modern value of 8×10^{18} molecules per cm^2. Note that the extent to which O_3 shields tropospheric H_2O can be strongly modulated by 3D dynamical effects (31), which we do not account for.

Like Fig. 2*A*, Fig. 2*B* also shows a transition between a 5×10^{-8} and 2×10^{-5} O_2 mixing ratio, but this model uses the modern outgassing fluxes for CO, H_2, H_2S, and SO_2 listed in Table 1 instead of presumptive Archean outgassing values. Also, at $t = 0$ y, we impose a stepwise increase of the O_2 flux from 10^{12} to 1.8×10^{12} molecules per $cm^2 \cdot s^{-1}$ while keeping the CH_4 flux/O_2 flux ratio at 0.45 (see *SI Appendix*, Fig. S1 for context). While the anoxic-to-oxic transition itself still occurs rapidly, the atmosphere simulated in Fig. 2*B* takes 60,000 y to reach the tipping point, which is much longer than the comparable O_2 transition shown in Fig. 2*A*.

The time required for O_2 to begin to rise in concentration is controlled by the reservoir of reducing gases, primarily CH_4, H_2, and CO, in the preoxygenated atmosphere. Big reservoirs of reducing gases slow the timescale of oxygenation, because reducing gases must be mostly removed before O_2 can increase. O_2 cannot increase while reducing gases are abundant, because large oxygen sinks from reactions with reducing gases prevent it. That is why 3,500 y elapse before O_2 begins to rise in Fig. 2*A*, and why 60,000 y elapse before O_2 rises in Fig. 2*B*. Fig. 2*B* starts with more reducing gases, which take longer to eradicate.

We can roughly estimate the time required for O_2 to begin to rise, with a back-of-the-envelope calculation of the rate at which reducing gases are eliminated from the anoxic atmosphere. The total reservoir of reducing gases in the preoxygenated atmosphere in O-equivalent units is

$$N_{\text{reducing}} = \sum_j N_j \alpha_j \approx -4N_{CH_4} - N_{CO} - N_{H_2}. \quad [2]$$

Here, N_{reducing} is the O-equivalent column abundance of reducing gases (O_{equiv} molecules per cm^2) which is equal to the sum of all reducing gases in the atmosphere (N_j) multiplied by α_j, the redox state of each gas. Redox state is a relative quantity that requires defining redox-neutral reference species. Following previous models of early Earth (5), we define H_2O, SO_2, CO_2, and N_2 as redox neutral, with the oxygen redox parameter $\alpha_O = +1$. Therefore, $\alpha_H = -0.5$, $\alpha_S = -2$, and

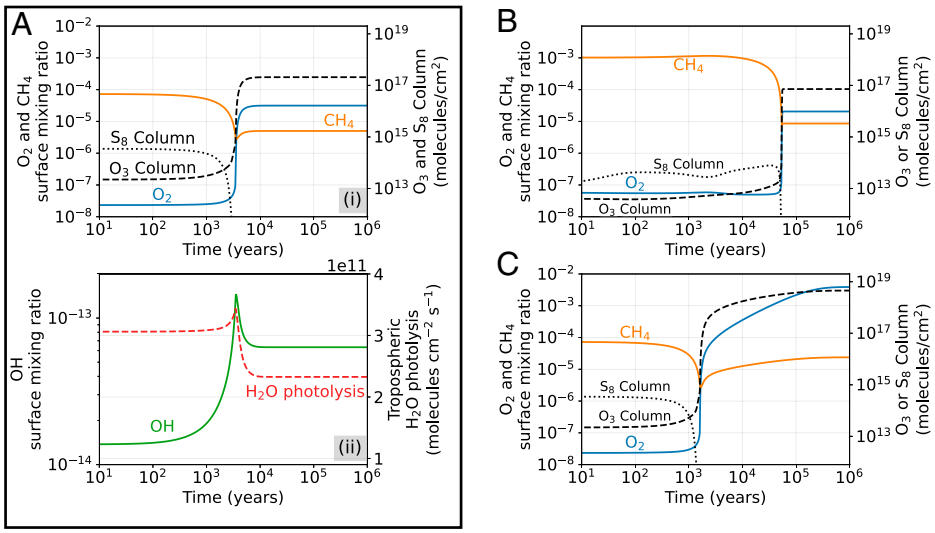

Fig. 2. Three models of anoxic-to-oxic transitions. (*A*) Atmospheric oxygenation caused by a step-wise decrease in the methane flux from 4.9×10^{11} to 4.7×10^{11} molecules per $cm^2 \cdot s^{-1}$ (orange arrow in Fig. 1). (*i*) Surface O_2 and CH_4 mixing ratios, and O_3 and S_8 column abundance over time; (*ii*) OH surface mixing ratio and tropospheric H_2O photolysis rate. (*B*) Transition caused by step-wise increase in the O_2 flux from 10^{12} to 1.8×10^{12} molecules per $cm^2 \cdot s^{-1}$ and a stepwise increase in the CH_4 flux to maintain constant CH_4 flux/O_2 flux = 0.45 (*SI Appendix*, Fig. S1). Transition in *C* results from a step-wise decrease in the CH_4 flux from 4.9×10^{11} to 4.5×10^{11} molecules per $cm^2 \cdot s^{-1}$ (black arrow in Fig. 1).

$\alpha_C = -2$, from redox stoichiometry of hydrogen, sulfur, and carbon, respectively. It then becomes straightforward to calculate the α_j for any molecule. For example, $\alpha_{CH_4} = \alpha_C + 4\alpha_H = -2 - 2 = -4$. For a more in-depth explanation of atmospheric redox, see section 3 in Harman et al. (32) or chapter 8 in Catling and Kasting (33). $N_{reducing}$ is approximately equal to the weighted sum of CH_4, H_2, and CO because these are the main reducing gases in an Archean Earth-like atmosphere.

The change in column abundance of reducing gases is the difference between the redox columns at the finial and initial atmospheric states.

$$\Delta N_{reducing} = N^{final}_{reducing} - N^{initial}_{reducing}. \quad [3]$$

In Fig. 2 *A* and *B*, we initiate the rise of oxygen by changing the surface flux of CH_4 and/or O_2 flux. We can quantify this flux perturbation in units of O_{equiv} molecules per square centimeter per second ($\Delta F_{O_{equiv}}$),

$$\begin{aligned}\Delta F_{O_{equiv}} &= \sum_i F_i^{final}\alpha_i - \sum_i F_i^{initial}\alpha_i \\ &= (2F^{final}_{O_2} - 4F^{final}_{CH_4}) - (2F^{initial}_{O_2} - 4F^{initial}_{CH_4}).\end{aligned} \quad [4]$$

Therefore, the time required to oxidize the reducing gases in the atmosphere and permit oxygen to begin rising is approximately

$$\tau_{oxy} = \left|\frac{\Delta N_{reducing}}{\Delta F_{O_{equiv}}}\right|. \quad [5]$$

Plugging in values for the O_2 transition in Fig. 2*B* yields $\tau_{oxy} = 2,900$ y, a value only slightly smaller than the 3,500 y predicted by the time-dependent photochemical model. For Fig. 2*B*, $\tau_{oxy} = 29,000$ y, which is about a factor of 2 smaller than the figure from 1D photochemistry. Our estimate is too small in this case because the reducing column and its destruction rate are not constant prior to the rise of oxygen (*SI Appendix*). This calculation illustrates that the time required for oxygen to begin rising, once a tipping point of fluxes is reached, mostly depends on the quantity of reducing gases in the preoxygenated atmosphere.

Fig. 2*C* shows a more substantial anoxic-to-oxic transition compared to simulations shown thus far (also see Movie S1). We start with the same steady-state atmosphere as in Fig. 2*A*, except we decrease the methane flux by twice as much at $t = 0$, from 4.9×10^{11} molecules per $cm^2 \cdot s^{-1}$ to 4.5×10^{11} molecules per $cm^2 \cdot s^{-1}$ instead of 4.7×10^{11} molecules per $cm^2 \cdot s^{-1}$ (we keep the surface O_2 flux constant at 10^{12} molecules per $cm^2 \cdot s^{-1}$). O_2 begins to rise and eliminates S_8 production after ~1,500 y, but O_2 will reach higher levels because of the lower CH_4 flux. It takes ~300,000 y for O_2 to reach its final steady-state abundance of 4×10^{-3} mixing ratio. While the switch from 10^{-8} to 10^{-5} O_2 mixing ratio remains as rapid as in Fig. 2*A*, the predicted increase in O_2 concentrations to 4×10^{-3} requires far longer. This timescale is roughly analogous to the time required to deplete H_2 and CH_4 reservoirs to allow O_2 to initially rise in concentration.

In summary, the timescale for O_2 to rise in concentration depends on the reservoir of redox gases in the atmosphere, and the magnitude of the perturbation to redox surface fluxes. For O_2 to rise from 10^{-8} to 10^{-5}, reducing gases must first be removed, which can take thousands to 10 thousands of years (Fig. 2 *A* and *B*). Increasing O_2 concentrations beyond 10^{-5} to near percentage levels requires filling a large O_2 reservoir, which occurs on 10^5-y timescales in our model run (Fig. 2*C*).

The Time Required for Deoxygenation. Here, we use our time-dependent photochemical model to address the controversy of the reversibility of the oxic transition (9, 11). Fig. 3 shows the reverse of model runs shown in Fig. 2. For each model run, we start with an atmosphere initially at a steady state at the end of the simulations shown in Fig. 2. Then we impose a stepwise change in the O_2 and CH_4 flux at $t = 0$ y to return the atmosphere to anoxia. The reversal of Fig. 2 takes ~700, 100, and 40,000 y, respectively, in comparison to the 3,500, 60,000, and 300,000 y required for oxygenation.

Like the timescale for oxygenation, the timescale of deoxygenation depends on the column abundance of redox-sensitive gases. In the previous section, we established that the timescale required for O_2 to begin to rise is merely the time required to deplete

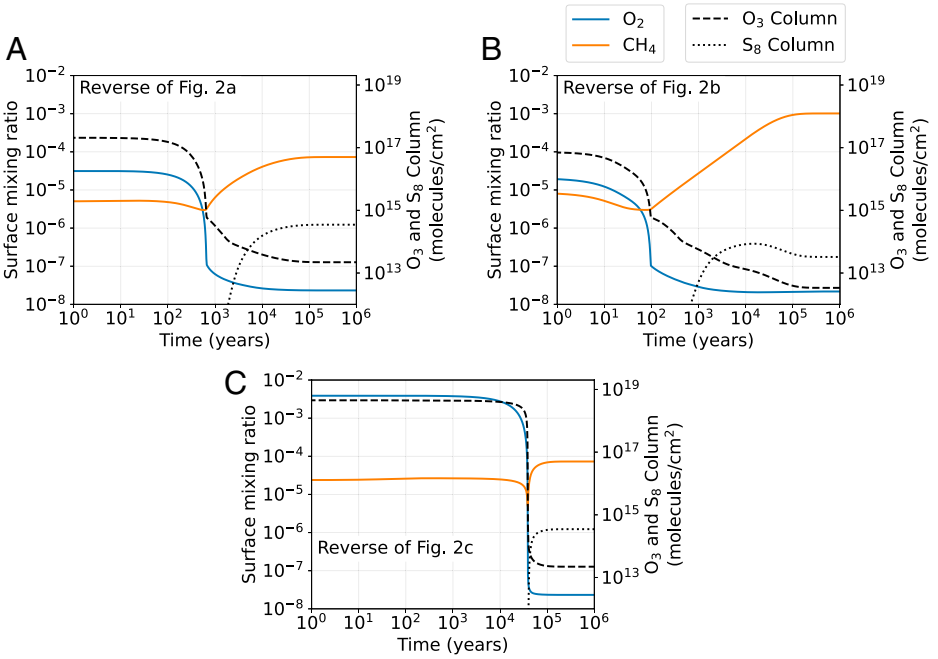

Fig. 3. (*A*–C) Simulated reversal of the oxic transitions shown in Fig. 2 *A*, *B*, and *C*, respectively. Each oxic-to-anoxic transition is caused by a stepwise change of the CH_4 flux and O_2 flux at $t = 0$ y.

the reservoirs of CH_4 and other reducing gases. Analogously, the timescale of deoxygenation is determined by the reservoir of O_2 and other oxidizing gases in the oxygenated atmosphere. The reversal shown in Fig. 3*B* starts with only 2×10^{-5} O_2, which can be depleted very quickly, allowing the return of an anoxic atmosphere. In contrast, the reversal shown in Fig. 3*C* takes 40,000 y because the atmosphere starts with 4×10^{-3} O_2, which takes longer to deplete.

The Stability of Post-GOE Atmospheric Oxygen. In the previous two sections, we show that reservoirs of redox gases, primarily methane and oxygen, give the atmosphere chemical inertia, controlling the timescale of O_2 changes. When reservoirs are big, for similar flux perturbations, the O_2 mixing ratio will change relatively slowly over time; however, when reservoirs are small, photochemistry permits rapid O_2 transitions. Therefore, the abundance of redox gases in an atmosphere is closely linked to the photochemical stability of oxygen.

Fig. 4*A* shows the steady-state inertial timescale of redox gases, τ_{inertia}, over the same axes as Fig. 1, which shows mixing ratios. τ_{inertia} is the sum of all redox gases in the atmospheric column (O-equivalent molecules per square centimeter), divided by a characteristic flux perturbation, which we take to be 10% of the O_2 flux,

$$\tau_{\text{inertia}} = \frac{N_{\text{redox}}}{F_{\text{redox perturb.}}} = \frac{\sum_i |\alpha_i| N_i}{0.1 \alpha_{O_2} F_{O_2}}. \quad [6]$$

We choose the characteristic flux perturbation to be 10% of the O_2 flux because it is the same order of magnitude as natural redox variations that occur on modern Earth during Milankovitch cycling (see *Discussion*). An upper limit for the characteristic flux perturbation would be 100% of the O_2 flux. This would decrease all τ_{inertia} values in Fig. 4*A* by a factor of 10, which would not change our interpretation. Since CH_4, CO, H_2, and O_2 are the most important redox gases, the numerator in Eq. **6** is well approximated by $4N_{CH_4} + N_{CO} + N_{H_2} + 2N_{O_2}$. Oxygen is the most prone to change for the smallest τ_{inertia} values, coinciding with O_2 mixing ratios between $\sim 10^{-8}$ and $\sim 10^{-5}$ shown in the whitish region of Fig. 4*A*.

The time-dependent photochemical models shown in Fig. 4 *B–D* illustrate the relationship between τ_{inertia} and O_2 instability. To produce Fig. 4*B*, we started with the steady-state atmosphere indicated on Fig. 4*A*, then imposed 17% amplitude oscillations to the CH_4 flux with a period of 10,000 y. This forcing had no perceptible effect on the 3×10^{-9} atmospheric O_2. A similar 20% CH_4 flux oscillation also did not significantly perturb an oxic atmosphere starting with 3×10^{-4} O_2 (Fig. 4*D*). However, just 5% CH_4 flux oscillations cause approximately four-orders-of-magnitude oscillations in surface oxygen concentrations for an incipiently oxic atmosphere starting with 3×10^{-7} O_2 (Fig. 4*C*). O_2 is most unstable where the abundance of all redox gases is smallest relative to a characteristic redox surface flux (the whitish area of Fig. 4*A*) between $\sim 10^{-8}$ and $\sim 10^{-5}$ O_2 mixing ratio. Stability continually increases outside of this range of O_2 concentrations.

While O_2 was relatively stable in the Fig. 4 *B* and *D* simulations, it does not mean these atmospheres and initial oxygen concentrations are stable to all atmospheric perturbations. The stability of any O_2 mixing ratio depends on the atmospheric forcings that are likely in nature. In *Discussion*, we argue that the CH_4 flux oscillations used in Fig. 4 are realistic because comparable fractional changes in the methane flux have occurred over the past 650,000 y.

Flux oscillations over timescales greater than ~ 10 y are required to significantly affect O_2 concentrations. Imposing 100% amplitude fluctuations to the CH_4 flux with a period of 1 y, starting with the same atmosphere as Fig. 4*C*, did not significantly alter the atmosphere over time. Atmospheres with between $\sim 10^{-8}$ and $\sim 10^{-5}$ O_2 contain some CH_4 and O_2, which gives the atmosphere inertia against annual to decadal change.

Discussion

Recently, Gregory et al. (16) computed photochemical steady-state atmospheres for a wide range of surface O_2 and CH_4 fluxes and found bistable O_2 concentrations. Their model allows steady-state atmospheres for O_2 concentrations below 6×10^{-7} and above 2×10^{-3} mixing ratio but admits few steady-state solutions in between. They hypothesized that feedbacks between O_2 and O_3 shielding eliminate most solutions with these intermediate O_2 concentrations. In contrast, our model can yield a steady-state solution with intermediate O_2 concentrations given the right constant surface flux boundary conditions [e.g., Fig. 2*B*; see also Gregory et al.'s (16) figure 8]. The difference might be

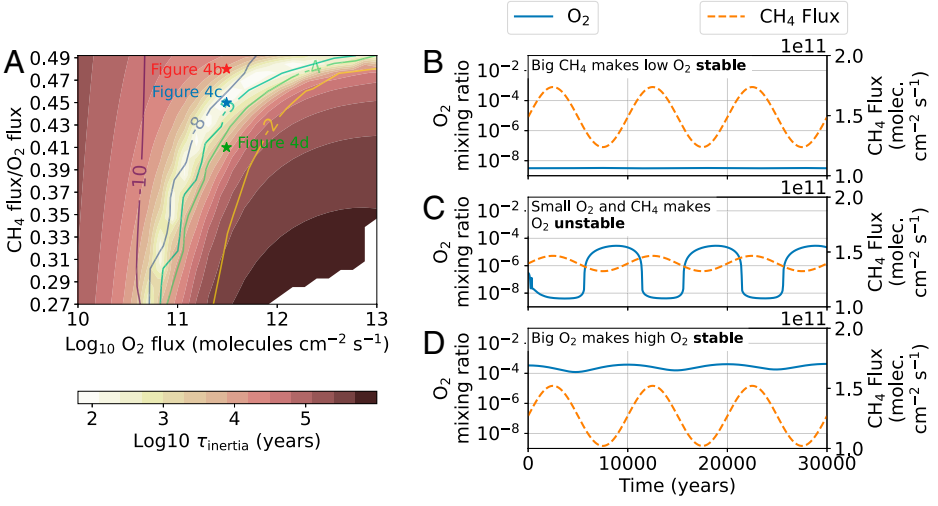

Fig. 4. The photochemical stability of O_2. Shading in *A* shows the steady-state inertial timescale of redox gases (Eq. **6**), and colored contours are the steady-state $\log_{10}$ surface O_2 mixing ratio (same as Fig. 1*A*). (*B–D*) Time-dependent photochemical simulations with oscillating CH_4 surface fluxes, each beginning with steady-state atmospheres indicated in *A*. O_2 stability is directly proportional to the column abundance of redox gases in the atmosphere.

caused by different steady-state convergence criteria, chemical reaction networks, boundary conditions, or a combination of these factors.

However, a photochemical steady state, for example, at 10^{-6} O_2 mixing ratio, does not mean that such an atmosphere is stable and realistic over 10^5- to 10^6-y timescales. Gas fluxes from Earth's surface can vary during these timescales and significantly change O_2 concentrations (*Results*).

For example, in the past 650,000 y, the biogenic methane flux has oscillated with an amplitude of 25% (6×10^9 molecules per $cm^2 \cdot s^{-1}$) and a 100,000-y period (34, 35). On modern Earth, methanogens in wetlands are a major source of atmospheric methane (36). Every 100,000 y, ice sheets have advanced and retreated, covering and uncovering wetlands, changing the CH_4 flux to the atmosphere. These ice ages and methane flux variations are in response to Milankovich cycles with characteristic periods between 20,000 and 100,000 y. This exact same methane oscillation would not have occurred in the Late Archean or Early Proterozoic because modern wetlands did not exist then, but a similar process involving microbial mats is conceivable.

Zhao et al. (37) modeled cyanobacterial mats on Proterozoic land, finding that they could have been a substantial CH_4 source to the atmosphere. Ice sheets covering and uncovering microbial mats could have affected global CH_4 fluxes. Fig. 4*C* illustrates the effect of 5% methane flux variations over Milankovitch timescales on an atmosphere starting with 3×10^{-7} O_2. O_2 oscillates nearly four orders of magnitude between $\sim 10^{-8}$ (anoxic) and $\sim 10^{-4}$ (oxic) (Fig. 4).

An oscillating methane flux is only one of many possible atmospheric perturbations. The Early Proterozoic geologic record preserves evidence of large igneous provinces (LIPs), or massive volcanic eruptions (8). In *SI Appendix*, we show that the H_2 and CO outgassed from a significant LIP eruption could cause the O_2 surface mixing ratio to drop from 2×10^{-5} to 4×10^{-9} in $\sim$100 y, causing a return to sulfur isotope MIF. In this simulation, we use the maximum LIP eruption rates reported in the literature (38). In addition to LIPs, a Snowball Earth event concurrent with the GOE would have presumably affected gases produced by the biosphere (10).

Constant surface gas fluxes from biology and volcanism for millions of years in the aftermath of the initial rise of O_2 are unlikely. Additionally, our photochemical modeling shows that, for atmospheres with transitional O_2 concentrations, relatively small atmospheric perturbations (e.g., a CH_4 flux change of 5%) over timescales as short as hundreds of years can cause O_2 to change by orders of magnitude (e.g., Fig. 3*B*). Therefore, substantial variability of O_2 during the GOE appears possible.

For these reasons, our photochemical modeling results are compatible with recently published evidence of fluctuating sulfur isotope MIF (8, 9) indicating that O_2 was unstable between 2.4 and 2.2 Ga. We find that shutoff of S_8 aerosol production, which is required to produce sulfur isotope MIF, occurs at $\sim 10^{-7}$ O_2 mixing ratio, a region of the parameter space where O_2 is prone to rapid change (Fig. 4). But, oxygen surface levels between $\sim 10^{-8}$ and $\sim 10^{-4}$ mixing ratio were likely unstable. Short period changes to the biosphere, or volcanic outgassing rates, could have caused order of magnitude O_2 changes over 100- to 100,000-y timescales. Occasionally, big perturbations to the atmosphere, such as an LIP, might have lowered O_2 concentrations enough for sulfur isotope MIF to reoccur. Note that the above explanation for the cause of O_2 oscillations prior to 2.2 Ga is complicated by S-MIF data presented in Izon et al. (11), which do not suggest the same O_2 variability found by Poulton et al. (9).

After 2.2 Ga, and during the mid-Proterozoic, sulfur isotope MIF never returned. Therefore, this time must have had O_2 concentrations large enough to prevent O_2 collapse. Our modeling shows that larger O_2 concentrations give the atmosphere chemical inertia, slowing atmospheric deoxygenation (Fig. 3). It is therefore challenging to reconcile our modeling results with the interpretation of Planavsky et al. (39), who used Proterozoic chromium isotopes to argue that O_2 could not have been larger than 2×10^{-4} mixing ratio. Such a small O_2 reservoir would have been unstable to LIP eruptions, or variations in the CH_4 flux from Milankovitch cycles (Fig. 4), which both have evidence of occurring in the mid-Proterozoic stratigraphic record (40–42). We conclude that, for stability, mid-Proterozoic O_2 levels should have exceeded $\sim 10^{-4}$. This conclusion is compatible with mid-Proterozoic Fe isotopes in ironstones, which suggest O_2 levels between approximately 2×10^{-4} and 2×10^{-3} mixing ratio (43).

Our results are not sensitive to the changing solar UV photon flux between the GOE ($\sim$2.4 Ga) and the mid-Proterozoic. Recalculating Fig. 1 using the solar UV flux at 1.3 Ga (44) results in surface O_2 and CH_4 surface mixing ratios within a factor of 2 of Fig. 1.

Our work also has implications for the most likely oxygen levels before the GOE. Johnson et al. (45) analyzed molybdenum isotopes in the Archean sedimentary record for signs of continental oxidative weathering. Their work is compatible with two end-member interpretations: 1) If Archean O_2 was evenly distributed over the globe, then the surface O_2 mixing ratio was $>3 \times 10^{-8}$ and $<2 \times 10^{-7}$, or 2) if O_2 accumulation was geographically restricted, then the O_2 surface flux was greater than 0.01 $Tmol \cdot y^{-1}$ (3×10^7 molecules per $cm^2 \cdot s^{-1}$). Our modeling suggests interpretation 1 is unlikely because we find that O_2 is likely unstable over geologic time for this range of oxygen levels.

In our modeling, we do not explicitly consider redox reservoirs in the oceans, sediments, crust, and mantle, for good reason. These reservoirs are coupled to the atmosphere and can modulate O_2 levels. However, the timescale of equilibration between the atmosphere and other redox reservoirs is often relatively long (e.g., 100 My for organic carbon in continental sediments), so we consider them to be approximately constant over the timescale of O_2 transitions ($<10^5$ y).

A caveat is that the coupling between redox reservoirs in the atmosphere, crust, or sediments might depend on atmospheric composition. An example is the pyrite oxidation rate, which depends on the partial pressure of oxygen (16). We do not explicitly consider such feedbacks, which could affect the timescale of changing O_2 levels.

An additional, related caveat is that our model does not consider biological feedbacks. The rise of O_2 would limit habitats for anaerobes, and permit more widespread aerobic respiration, potentially dropping the CH_4 flux/O_2 flux ratio farther than we have modeled here. Also, a stronger ozone UV shield would make new habitats for cyanobacteria and allow the expansion of life on land, promoting chemical and oxidative weathering. All these changes, which we do not explicitly model, would modulate oxygen levels. In this article, we impose changes in the CH_4 and O_2 flux that are supposed to be representative of a changing biosphere, but a better model would determine more realistic changes in gas fluxes by directly coupling 1D photochemistry and biology.

Conclusions

Our time-dependent photochemical modeling of the GOE suggests that oxygen can rise and fall over geologically short periods of time. For an anoxic-to-oxic transition, once a tipping point of imbalanced redox fluxes is reached, the reservoir of reducing gases in the atmosphere must be eliminated before O_2 can begin to rise. This takes hundreds to 10 thousands of years. O_2 accumulation to just hundredths or tenths of percent levels requires filling a large O_2 reservoir, which may occur on a 10^5-y timescale. Atmospheric deoxygenation occurs over similar periods of time, mainly controlled by the magnitude of the initial O_2 abundance.

We also find O_2 instability, especially for mixing ratios between $\sim 10^{-8}$ and $\sim 10^{-5}$. For these O_2 concentrations, photochemistry demands that both CH_4 and O_2 be relatively small in concentration. This small reservoir of redox-sensitive gases permits rapid changes to the atmosphere's redox state. For example, for an atmosphere starting with 3×10^{-7} O_2, 5% amplitude oscillations to the methane flux with a period of 10,000 y cause oxygen to fluctuate four orders of magnitude between anoxic and oxic. Additionally, we show that a LIP eruption could cause the collapse of O_2 and the return of sulfur isotope MIF for an atmosphere starting with 2×10^{-5} O_2 mixing ratio (*SI Appendix*).

We emphasize that the short-term (10^2 to 10^5 y) variability in O_2 levels considered here occurred on the backdrop of the billion-year oxidation of the crust and mantle, and long-term organic burial, which are argued to be the ultimate causes of the rise of oxygen on Earth (e.g., ref. 20).

Overall, our modeling is compatible with, but does not prove, proposed geologic evidence for fluctuating and unstable atmospheric O_2 after the initial rise of oxygen 2.4 billion years ago. A single, unidirectional, oxidation event remains plausible, although it would require strong and perhaps biological feedbacks promoting permanent substantial changes in the global CH_4 flux/O_2 flux ratio. While this is evident between the Archean (CH_4 flux/O_2 flux ≈ 0.5) and modern (CH_4 flux/O_2 flux ≈ 0.1) biospheres, the dynamics of the Proterozoic biosphere remain largely unexplored. Also, our results suggest that a stable, post-GOE, mid-Proterozoic atmosphere would need an O_2 mixing ratio exceeding a value in the 10^{-4} to 10^{-3} range.

Materials and Methods

To investigate the transition between an anoxic and oxygen-rich Earth, we use a photochemical model with one spatial dimension of altitude, approximating a global average vertical profile. One-dimensional photochemical models are typically governed by a simplification of the continuity equation for molecules,

$$\frac{\partial n_i}{\partial t} = -\frac{\partial}{\partial z}\Phi_i + P_i - L_i + R_{\text{i, rainout}} + Q_{\text{i, lightning}}. \quad \textbf{[7]}$$

Table 2 defines all the variables and their units. Here, the flux (Φ_i) is given by

$$\Phi_i = -Kn\frac{\partial}{\partial z}\left(\frac{n_i}{n}\right) - D_i n_i\left(\frac{1}{n_i}\frac{\partial n_i}{\partial z} + \frac{1}{H_i} + \frac{1+\alpha_{\text{Ti}}}{T}\frac{\partial T}{\partial z}\right).$$

The above system of partial differential equations (PDEs) describes how the number density (n_i) of each chemical species i changes over altitude and time.

In our photochemical model, we solve a simplified version of Eq. **7** which assumes that the total number density does not change over time ($\partial n/\partial t \approx 0$). This assumption is valid for atmospheric transitions which maintain approximately constant surface pressure and atmospheric temperature. The continuity equations can then be written in terms of mixing ratios (f_i) instead of number densities (see Appendix B.1 in ref. 33 for a derivation),

$$\frac{\partial f_i}{\partial t} = -\frac{1}{n}\frac{\partial}{\partial z}\Phi_i + \frac{P_i}{n} - \frac{L_i}{n} - \frac{R_{\text{i, rainout}}}{n} + \frac{Q_{\text{i, lightning}}}{n} \quad \textbf{[8]}$$

$$\Phi_i = -(K + D_i)\, n\frac{\partial f_i}{\partial z} - \zeta_i n f_i \quad \textbf{[9]}$$

$$\zeta_i = D_i\left(\frac{1}{H_i} - \frac{1}{H_a} + \frac{\alpha_{\text{Ti}}}{T}\frac{\partial T}{\partial z}\right). \quad \textbf{[10]}$$

To approximate Eq. **8**, the model replaces the spatial derivatives with finite difference approximations, turning the system of PDEs into a larger system of ordinary differential equations (ODEs). This is the "method of lines" approach to solving a PDE. Catling and Kasting (33), their Appendix B.2, provides a detailed description of how to do this with Eq. **8**; therefore, we will omit a detailed description here, except to point out a sign error. The first two terms for the equation for B in their equation B.16 should have minus signs instead of plus signs.

Table 2. Variables in Eq. 7

Variable	Definition	Units
f_i	Mixing ratio of species i	Dimensionless
n_i	Number density of species i	Molecules per cubic centimeter
z	Altitude	Centimeters
t	Time	Seconds
n	Total number density	Molecules per cubic centimeter
P_i	Total chemical production of species i	Molecules per cubic centimeter per second
L_i	Total chemical loss of species i	Molecules per cubic centimeter per second
$R_{\text{i, rainout}}$	Production and loss of species i from rainout	Molecules per cubic centimeter per second
$Q_{\text{i, lightning}}$	Production and loss of species i from lightning	Molecules per cubic centimeter per second
Φ_i	Vertical flux of species i	Molecules per square centimeter per second
K	Eddy diffusion coefficient	Square centimeters per second
D_i	Molecular diffusion coefficient	Square centimeters per second
H_i	$= N_a$kT/$\mu_i g$, The scale heights of species i	Centimeters
H_a	$= N_a$kT/$\overline{\mu} g$, The average scale height.	Centimeters
N_a	Avogadro's number	Molecules per mole
k	Boltzmann's constant	Ergs per kelvin
μ	Molar mass. $\overline{\mu}$ is mean molar mass of the atmosphere, and μ_i is the molar mass of species i	Grams per mole
g	Gravitational acceleration	Centimeters per square second
α_{Ti}	Thermal diffusion coefficient of species i. We neglect this term ($\alpha_{\text{Ti}} = 0$)	Dimensionless
T	Temperature	Kelvins

The system of ODEs derived from finite differencing Eq. **8** can be evolved forward in time with numerical integration. However, the photochemical ODEs are "stiff," meaning that some dependent variables (i.e., the mixing ratios) change much more quickly than others. For example, in the modern atmosphere, OH typically has a chemical lifetime of about 1 s, while CH_4 has a chemical lifetime of $\sim$10 y. Stiff equations require special, high-stability, "implicit" integration methods. For more details on stiff equations and the implicit methods used to solve them, see ref. 46.

Often, we solve for steady states of the photochemical continuity equation ($\partial f_i/\partial t = 0$). To find steady states, we begin with some initial atmospheric composition, then integrate Eq. **8** forward in time until the atmosphere ceases to change, that is, a steady state is reached. The assumption of photochemical steady state is approximately valid for most periods of Earth's history, because the atmosphere changes slowly enough to be in a quasi-steady state.

However, the Paleoproterozoic rise of O_2 was a relatively fast atmospheric transition that is not well modeled as a photochemical steady-state process. Therefore, describing it requires accurately solving the continuity equation over time.

To model the photochemistry of the GOE, we modified the photochemical model contained within the Atmos modeling suite (described in Appendix B of ref. 33) so that it can accurately solve the time-dependent behavior of Eq. **8**. We call the modified version of the model PhotochemPy. Instead of using a Backward Euler as in Atmos, we used CVODE BDF ODE solver from Sundials Computing (47). CVODE BDF is an implementation of the backward differential formulas (BDF) and is a gold standard for solving large chemical kinetics problems. For details, see *SI Appendix*.

PhotochemPy is open source under a Massachusetts Institute of Technology license. The version of the code (v0.2.14) used in this paper and the corresponding Python scripts to reproduce work done in this article are at https://zenodo.org/record/6824092. However, the most up-to-date version of the code can be found at the following GitHub link: https://github.com/Nicholaswogan/PhotochemPy.

Data, Materials, and Software Availability. Source code has been deposited in Zenodo (https://zenodo.org/record/6824093#.Ys3KuOzMKCc) (48). PhotochemPy code and the corresponding Python scripts are available at https://zenodo.org/record/6824092. The most up-to-date code is available at https://github.com/Nicholaswogan/PhotochemPy (49).

ACKNOWLEDGMENTS. We thank Joshua Krissansen-Totton for reading an early version of the article and providing knowledgeable and constructive comments and conversations. We also thank Daniel R. Shapero and Sandra Bastelberger for conversations that helped us construct the time-dependent photochemical model used in this paper. Additionally, we thank Ben Uveges for improving our understanding of the ancient sulfur isotope record and Andrew Hoffman for informing us that ice ages can cause variations in atmospheric methane. The manuscript was also improved by comments from three anonymous reviewers. N.F.W. and D.C.C. were supported by the Simons Collaboration on Origin of Life Grant 511570 (to D.C.C.). Also, N.F.W., D.C.C., and K.J.Z. were supported by NASA Astrobiology Program Grant 80NSSC18K0829 and benefited from participation in the NASA Nexus for Exoplanet Systems Science research coordination network. N.F.W. and D.C.C. also acknowledge support from Sloan Foundation Grant G-2021-14194. M.W.C. was supported by the European Research Council under the European Union's Horizon 2020 Research and Innovation program (Grant 678812 awarded to M.W.C.).

Author affiliations: [a]Department of Earth and Space Sciences, University of Washington, Seattle, WA 98195; [b]Virtual Planetary Laboratory, University of Washington, Seattle, WA 98195; [c]Space Science Division, NASA Ames Research Center, Moffett Field, CA 94035; [d]School of Earth and Environmental Sciences, University of St. Andrews, St. Andrews KY16 9AJ, United Kingdom; and [e]Blue Marble Space Institute of Science, Seattle, WA 98104

1. V. S. Meadows *et al.*, Exoplanet biosignatures: Understanding oxygen as a biosignature in the context of its environment. *Astrobiology* **18**, 630–662 (2018).
2. D. C. Catling, C. R. Glein, K. J. Zahnle, C. P. McKay, Why O2 is required by complex life on habitable planets and the concept of planetary "oxygenation time." *Astrobiology* **5**, 415–438 (2005).
3. D. C. Catling, K. J. Zahnle, The Archean atmosphere. *Sci. Adv.* **6**, eaax1420 (2020).
4. M. R. Warke *et al.*, The great oxidation event preceded a paleoproterozoic "snowball Earth." *Proc. Natl. Acad. Sci. U.S.A.* **117**, 13314–13320 (2020).
5. K. Zahnle, M. Claire, D. Catling, The loss of mass-independent fractionation in sulfur due to a palaeoproterozoic collapse of atmospheric methane. *Geobiology* **4**, 271–283 (2006).
6. A. A. Pavlov, J. F. Kasting, Mass-independent fractionation of sulfur isotopes in Archean sediments: Strong evidence for an anoxic Archean atmosphere. *Astrobiology* **2**, 27–41 (2002).
7. J. Farquhar, H. Bao, M. Thiemens, Atmospheric influence of Earth's earliest sulfur cycle. *Science* **289**, 756–759 (2000).
8. A. P. Gumsley *et al.*, Timing and tempo of the Great Oxidation Event. *Proc. Natl. Acad. Sci. U.S.A.* **114**, 1811–1816 (2017).
9. S. W. Poulton *et al.*, A 200-million-year delay in permanent atmospheric oxygenation. *Nature* **592**, 232–236 (2021).
10. B. Rasmussen, A. Bekker, I. R. Fletcher, Correlation of paleoproterozoic glaciations based on U–Pb zircon ages for tuff beds in the Transvaal and Huronian supergroups. *Earth Planet. Sci. Lett.* **382**, 173–180 (2013).
11. G. Izon *et al.*, Bulk and grain-scale minor sulfur isotope data reveal complexities in the dynamics of Earth's oxygenation. *Proc. Natl. Acad. Sci. U.S.A.* **119**, e2025606119 (2022).
12. C. Goldblatt, T. M. Lenton, A. J. Watson, Bistability of atmospheric oxygen and the great oxidation. *Nature* **443**, 683–686 (2006).
13. J. Kasting, T. Donahue, The evolution of atmospheric ozone. *J. Geophys. Res. Oceans* **85**, 3255–3263 (1980).
14. A. Segura *et al.*, Ozone concentrations and ultraviolet fluxes on Earth-like planets around other stars. *Astrobiology* **3**, 689–708 (2003).
15. A. A. Pavlov, L. L. Brown, J. F. Kasting, UV shielding of NH_3 and O_2 by organic hazes in the Archean atmosphere. *J. Geophys. Res. Planets* **106**, 23267–23287 (2001).
16. B. S. Gregory, M. W. Claire, S. Rugheimer, Photochemical modelling of atmospheric oxygen levels confirms two stable states. *Earth Planet. Sci. Lett.* **561**, 116818 (2021).
17. M. W. Claire *et al.*, Modeling the signature of sulfur mass-independent fractionation produced in the Archean atmosphere. *Geochim. Cosmochim. Acta* **141**, 365–380 (2014).
18. G. Izon *et al.*, Biological regulation of atmospheric chemistry en route to planetary oxygenation. *Proc. Natl. Acad. Sci. U.S.A.* **114**, E2571–E2579 (2017).
19. F. Kurzweil *et al.*, Atmospheric sulfur rearrangement 2.7 billion years ago: Evidence for oxygenic photosynthesis. *Earth Planet. Sci. Lett.* **366**, 17–26 (2013).
20. D. C. Catling, K. J. Zahnle, C. McKay, Biogenic methane, hydrogen escape, and the irreversible oxidation of early Earth. *Science* **293**, 839–843 (2001).
21. M. W. Claire, D. C. Catling, K. J. Zahnle, Biogeochemical modelling of the rise in atmospheric oxygen. *Geobiology* **4**, 239–269 (2006).
22. S. Kadoya, D. C. Catling, R. W. Nicklas, I. S. Puchtel, A. D. Anbar, Mantle data imply a decline of oxidizable volcanic gases could have triggered the Great Oxidation. *Nat. Commun.* **11**, 2774 (2020).
23. H. D. Holland, Volcanic gases, black smokers, and the Great Oxidation event. *Geochim. Cosmochim. Acta* **66**, 3811–3826 (2002).
24. J. F. Kasting, D. H. Eggler, S. P. Raeburn, Mantle redox evolution and the oxidation state of the Archean atmosphere. *J. Geol.* **101**, 245–257 (1993).
25. D. E. Canfield, K. S. Habicht, B. Thamdrup, The Archean sulfur cycle and the early history of atmospheric oxygen. *Science* **288**, 658–661 (2000).
26. D. C. Catling, M. W. Claire, K. J. Zahnle, Anaerobic methanotrophy and the rise of atmospheric oxygen. *Philos. Trans. R. Soc. Math. Phys. Eng. Sci.* **365**, 1867–1888 (2007).
27. S. L. Olson, C. T. Reinhard, T. W. Lyons, Limited role for methane in the mid-Proterozoic greenhouse. *Proc. Natl. Acad. Sci. U.S.A.* **113**, 11447–11452 (2016).
28. T. A. Laakso, D. P. Schrag, A small marine biosphere in the Proterozoic. *Geobiology* **17**, 161–171 (2019).
29. M. A. Kipp, J. Krissansen-Totton, D. C. Catling, High organic burial efficiency is required to explain mass balance in Earth's early carbon cycle. *Glob. Biogeochem. Cycles* **35**, e2020GB006707 (2021).
30. J. Krissansen-Totton, G. N. Arney, D. C. Catling, Constraining the climate and ocean pH of the early Earth with a geological carbon cycle model. *Proc. Natl. Acad. Sci. U.S.A.* **115**, 4105–4110 (2018).
31. G. J. Cooke, D. R. Marsh, C. Walsh, B. Black, J. F. Lamarque, A revised lower estimate of ozone columns during Earth's oxygenated history. *R. Soc. Open Sci.* **9**, 211165 (2022).
32. C. Harman, E. Schwieterman, J. C. Schottelkotte, J. Kasting, Abiotic O_2 levels on planets around F, G, K, and M stars: Possible false positives for life? *Astrophys. J.* **812**, 137 (2015).
33. D. C. Catling, J. F. Kasting, *Atmospheric Evolution on Inhabited and Lifeless Worlds* (Cambridge University Press, 2017).
34. P. O. Hopcroft, P. J. Valdes, J. O. Kaplan, Bayesian analysis of the glacial-interglacial methane increase constrained by stable isotopes and earth system modeling. *Geophys. Res. Lett.* **45**, 3653–3663 (2018).
35. R. Spahni *et al.*, Atmospheric methane and nitrous oxide of the Late Pleistocene from Antarctic ice cores. *Science* **310**, 1317–1321 (2005).
36. J. G. Canadell *et al.*, "Global carbon and other biogeochemical cycles and feedbacks" in *Climate Change 2021: The Physical Science Basis*, V. Masson-Delmotte et al., Eds. (Cambridge University Press, 2021), chap. 5.
37. M. Zhao, C. T. Reinhard, N. Planavsky, Terrestrial methane fluxes and Proterozoic climate. *Geology* **46**, 139–142 (2018).
38. S. E. Bryan *et al.*, The largest volcanic eruptions on Earth. *Earth Sci. Rev.* **102**, 207–229 (2010).
39. N. J. Planavsky *et al.*, Low mid-Proterozoic atmospheric oxygen levels and the delayed rise of animals. *Science* **346**, 635–638 (2014).
40. S. Zhang *et al.*, Orbital forcing of climate 1.4 billion years ago. *Proc. Natl. Acad. Sci. U.S.A.* **112**, E1406–E1413 (2015).
41. S. R. Meyers, A. Malinverno, Proterozoic Milankovitch cycles and the history of the solar system. *Proc. Natl. Acad. Sci. U.S.A.* **115**, 6363–6368 (2018).
42. A. LeCheminant, L. Heaman, Mackenzie igneous events, Canada: Middle proterozoic hotspot magmatism associated with ocean opening. *Earth Planet. Sci. Lett.* **96**, 38–48 (1989).
43. C. Wang *et al.*, Strong evidence for a weakly oxygenated ocean-atmosphere system during the Proterozoic. *Proc. Natl. Acad. Sci. U.S.A.* **119**, e2116101119 (2022).
44. M. W. Claire *et al.*, The evolution of solar flux from 0.1 nm to 160 μmm: Quantitative estimates for planetary studies. *Astrophys. J.* **757**, 95 (2012).
45. A. C. Johnson *et al.*, Reconciling evidence of oxidative weathering and atmospheric anoxia on Archean Earth. *Sci. Adv.* **7**, eabj0108 (2021).
46. E. Hairer, G. Wanner, *Solving Ordinary Differential Equations II* (Springer, Berlin, 1996).
47. A. C. Hindmarsh *et al.*, Sundials: Suite of nonlinear and differential/algebraic equation solvers. *ACM Trans. Math. Softw.* **31**, 363–396 (2005).
48. N. Wogan, D. Catling, K. Zhanle, M. Claire, PhotochemPy v0.2.14 and code for reproducing figures in Wogan et al. Zenodo. https://zenodo.org/record/6824093#.Yv_REezMKCc. Deposited 12 July 2022.
49. N. Wogan, PhotochemPy. GitHub. https://github.com/Nicholaswogan/PhotochemPy. Deposited 20 April 2022.

PNAS
www.pnas.org

Supplementary Information for

Rapid Timescale for an Oxic Transition During the Great Oxidation Event and the Instability of Low Atmospheric O_2

Nicholas F. Wogan, David C. Catling, Kevin J. Zahnle, and Mark W. Claire

Nicholas Wogan
E-mail: wogan@uw.edu

This PDF file includes:

Supplementary text
Figs. S1 to S4 (not allowed for Brief Reports)
Legend for Movie S1
SI References

Other supplementary materials for this manuscript include the following:

Movie S1

Supporting Information Text

All Great Oxidation Event (GOE) simulations use the solar spectrum at 2.4 Ga, calculated with methods described in Claire et al. (2012) (1). We also always include chemical rainout and NO production from lightning. 95% of steady state simulations conserve redox to a factor better than 10^{-6}. 3% of models, all with $> 0.1\%$ steady-state O_2, conserve redox to a factor of $\sim 10^{-3}$. Figure S1 shows results from steady-state photochemical simulations over the same parameter space as Figure 1 (main text), except using the "Modern Values" fluxes from Table 1 in the main text. Figure S2 shows assumed eddy diffusion and temperature profiles.

Estimating the timescale of the rise of O_2

In the results section of the main text, we estimated the timescale for the rise of O_2 using the following equation:

$$\tau_{\rm oxy} = \left| \frac{\Delta N_{\rm reducing}}{\Delta F_{\rm O_{equiv}}} \right| \quad [1]$$

Applying this equation to the Figure 2b (main text) simulation:

$$\begin{aligned} \Delta F_{\rm O_{equiv}} &= (2F^{\rm final}_{\rm O_2} - 4F^{\rm final}_{\rm CH_4}) - (2F^{\rm initial}_{\rm O_2} - 4F^{\rm initial}_{\rm CH_4}) \\ &= (2(1.8\times10^{12}) - 4(8.1\times10^{11})) - (2(1.0\times10^{12}) - 4(4.5\times10^{11})) \\ &= 1.6\times10^{11} \text{ molecules cm}^{-2}\text{ s}^{-1} \end{aligned} \quad [2]$$

$$\tau_{\rm oxy} = \left| \frac{\Delta N_{\rm reducing}}{\Delta F_{\rm O_{equiv}}} \right| = \left| \frac{1.47\times10^{23}}{1.6\times10^{11}} \right| = 9.8\times10^{11} \text{ s} = 29,000 \text{ years} \quad [3]$$

This estimation is about a factor of two smaller than the ∼60,000 years predicted by our time-dependent photochemical model.

Figure S3 shows the column of reducing gases and its destruction rate during the Figure 2b simulation. Our estimation for the timescale of oxygenation (Equation Eq. (3)) is off by a factor of two because the reducing column evolves over time, and our estimation of its destruction rate ($\Delta F_{\rm O_{equiv}}$) is too large. In the photochemical model, chemistry and transport does not permit a reducing column destruction rates identical to the imposed change in redox fluxes at the surface (1.6×10^{11} O molecules cm^{-2} s^{-1}).

A Large Igneous Province may have destabilized atmospheric oxygen

Here, we show that the H_2 and CO outgassing from large igneous provinces (LIPs), or massive volcanic eruptions, could have potentially caused the collapse of transitional O_2 concentrations ($\sim 10^{-8}$ to $\sim 10^{-4}$ mixing ratio).

To compute H_2 and CO outgassing rates from LIPs, we use the outgassing model described in (2). To briefly summarize, the model estimates the composition of gas bubbles suspended in magma just prior to release into the overlying atmosphere or ocean. Gas composition is computed by solving a system of equations including solubility relationships for H_2O and CO_2, gas-phase equilibrium relationships, and mass conservation of hydrogen and carbon. The model has five inputs: Magma oxygen fugacity, temperature, and overburden pressure, and the H_2O and CO_2 mass fractions ($m^{\rm tot}_{\rm H_2O}$, and $m^{\rm tot}_{\rm CO_2}$) in the magma before degassing occurs. For LIPs, we assume a magma oxygen fugacity one log-unit below the fayalite-magnetite-quartz mineral redox buffer (i.e. ΔFMQ-1) following Archean proxies (3). See Chapter 7 in (4) for a description of the fayalite-magnetite-quartz redox buffer. Additionally, we use $m^{\rm tot}_{\rm H_2O} = 0.5$ wt% and $m^{\rm tot}_{\rm CO_2} = 0.05$ wt% which agrees with estimates of LIP volatile concentrations (5). Finally, we take the degassing temperature and pressure to be 1473 K and 1 bar, respectfully. With these inputs, our outgassing model predicts 1.6×10^{-2} mol H_2/kg magma and 1.7×10^{-3} mol CO/kg magma.

Converting gas production rates (e.g. mol H_2/kg magma) into gas fluxes to the atmosphere requires estimations of magma eruption rates during LIPs. Basaltic LIPs typically last several million years and cumulatively produce $> 3\times10^{18}$ kg magma (6). This magma is release over 10s to 100s of eruptions each lasting several years to 10s of years with eruptions rates between 3×10^{13} to 3×10^{15} kg magma yr^{-1} (7). Multiplying these eruption rates by calculated gas production yields H_2 fluxes between 1.9×10^{9} and 1.9×10^{11} molecules cm^{-2} s^{-1} and CO fluxes between 2.0×10^{8} and 2.0×10^{10} molecules cm^{-2} s^{-1}.

The time-dependent photochemical simulation shown in Figure S4 shows how atmospheric O_2 responds to maximum LIP H_2 and CO outgassing scenario. The simulation starts with an atmosphere initially at equilibrium, then at $t = 0$ years, we increase the H_2 and CO outgassing fluxes by 1.9×10^{11} and 2.0×10^{10} molecules cm^{-2} s^{-1}, respectfully. O_2 drops from 2×10^{-5} to 4×10^{-9} in 100 years. Basaltic LIP eruptions can last for 10s of years (7), so a 100 year eruption, which is required to cause O_2 to collapse, is within the realm of possibility. However, the period of anoxia would likely be maintained for only a few hundred years, until the eruption ceased. Several periods of anoxia, each corresponding to a significant eruption, might occur during an entire several-million-year LIP event.

It is unclear whether a 100 year period of anoxia is detectable in the geologic record of multiple sulfur isotopes. A single sample from the sedimentary record might represent a period of time greater than 100 years, thus containing sulfur from both an oxic and anoxic atmosphere, diluting the S-MIF signal. Evaluating the detectability of short-term anoxia in the sedimentary record of sulfur isotopes is an interesting target for future work coupling in-situ and bulk rock measurements (8).

LIPs may have additional effects on the atmosphere that we are not accounting for in the above calculations. For example, increased Cl outgassing could catalyze O_3 and CH_4 destruction (e.g. $Cl + O_3 \rightarrow ClO + O_2$ and $Cl + CH_4 \rightarrow HCl + CH_3$), which could have a non-trivial effect on the O_2 concentration.

CVODE numerical integrator

To accurately track atmospheric chemistry over time with our photochemical model, we use the CVODE BDF ODE solver. The reasons CVODE BDF can reliably solve the continuity equation over time are its method of timestep selection and local error control. At each timestep, CVODE estimates the local error that will be introduced with a given timestep size. If the local error is less than the accuracy requirement specified by the user, then the step is accepted and the integration proceeds. Otherwise, the step is rejected, and CVODE retries with a smaller timestep. This general approach is standard in production-grade ODE solvers and will guarantee that each step introduces less local error than that specified by the user (9). The time stepping approach in the older versions of the *Atmos* photochemical model does not estimate the local error introduced with each step, and thus the inaccuracies introduced with integration. This makes it very challenging to determine whether an integration is a good approximation of the true solution or not.

CVODE BDF is also several times faster, depending on the problem, than the backward Euler implementation in older versions of *Atmos*. CVODE uses implementations of the backward differential formulae that are up to 5^{th} order accurate. Backward Euler is 1^{st} order accurate. Higher order ODE integration methods are generally faster because they can take larger timesteps compared to lower order methods while achieving the same accuracy. CVODE also only computes a new Jacobian every few steps when a new one is needed, while the original integrator in *Atmos* computed a Jacobian every single timestep. Jacobians are expensive to compute, thus fewer Jacobian calculations means a faster program.

In addition to implementing time-accurate integration, PhotochemPy is distinct from *Atmos* in a several other ways. The list below highlights the most important differences.

- We restructured the Fortran 77 code using modern Fortran practices. Refactoring in modern Fortran allows more program bugs to be caught during compilation.
- We significantly reduced hard-coding in the model, increasing model generality. PhotochemPy can model vastly different atmospheres such as Saturn, Earth, or Mars with minimal parameter changes which are clear to the user, and not buried deep in the source code.
- We also used the Numpy F2PY tool to generate a deep Python interface to the compiled Fortran (10). This enables easy parallel photochemical integrations using Python multiprocessing tools.
- We introduced extensive call-back errors, which significantly reduces the chances of unnoticed bugs, like a reaction rate which is entered incorrectly.

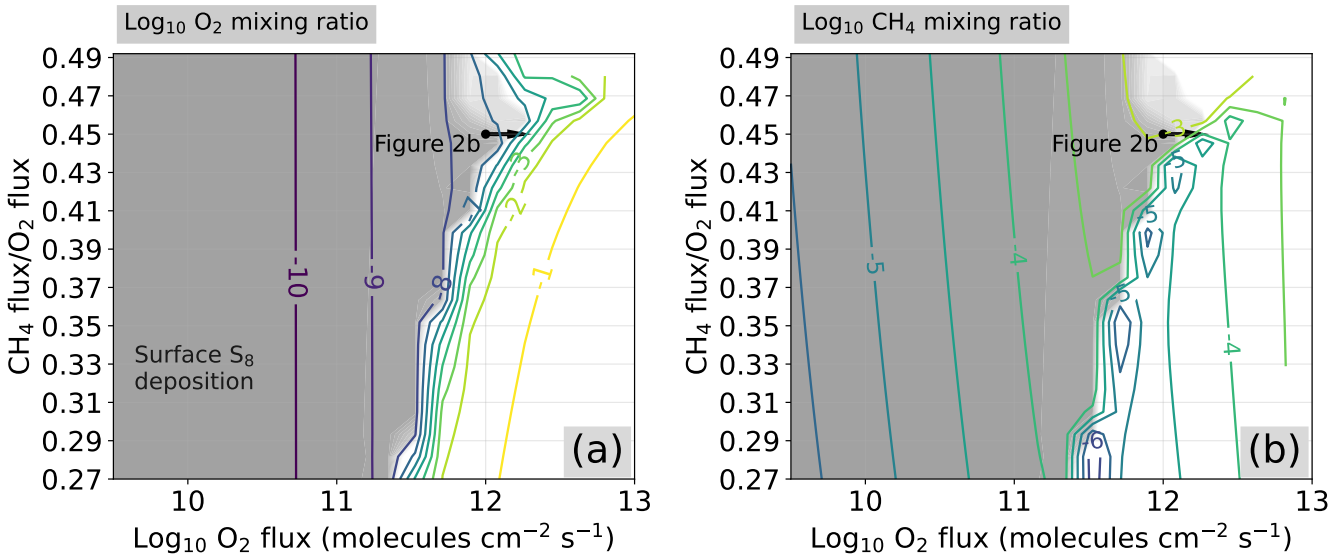

Fig. S1. Identical to Figure 1 in the main text, except we use the "Modern Values" surface fluxes in Table 1 in the main text. The time-dependent photochemical simulation shown in Figure 2b (main text), is indicated with a black arrow.

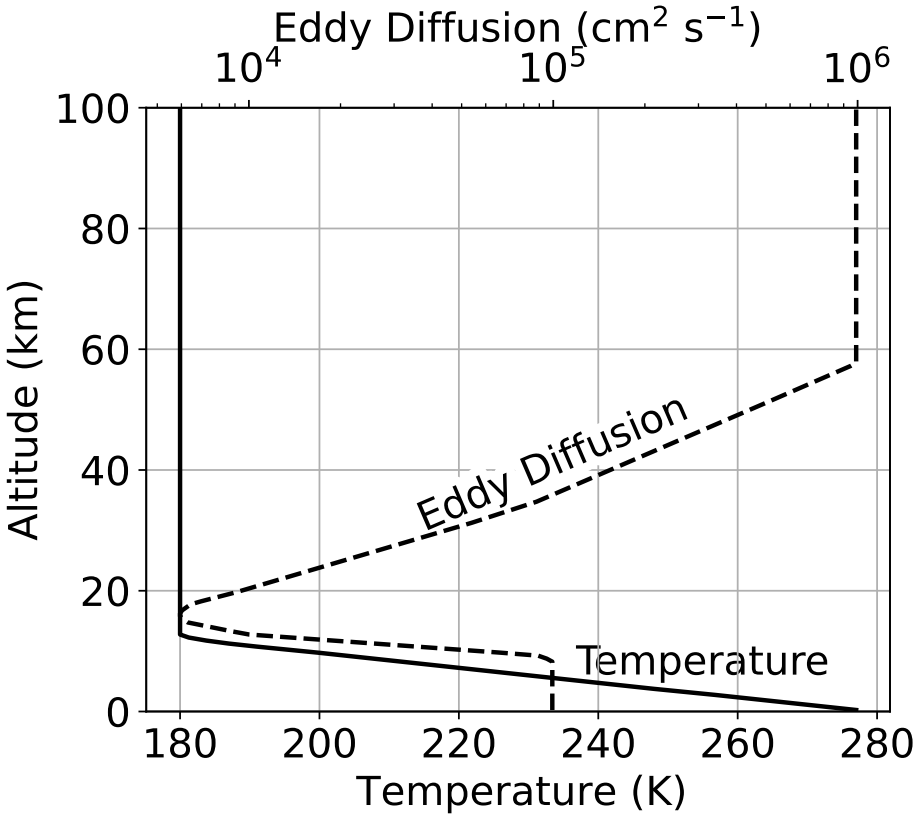

Fig. S2. The temperature and eddy diffusion used for every simulation.

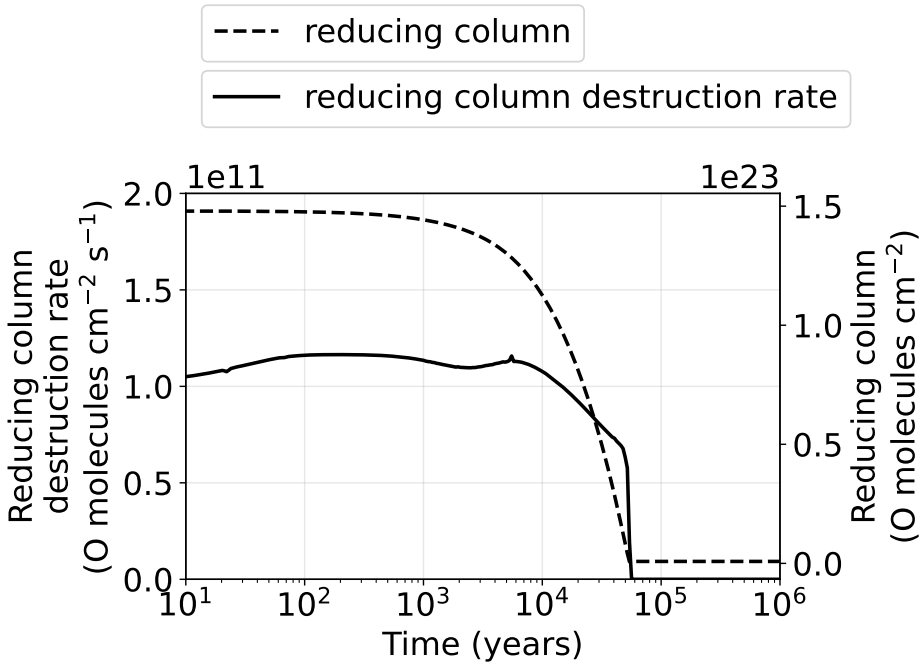

Fig. S3. Reducing gas column and its destruction rate for the simulation shown in Figure 2b.

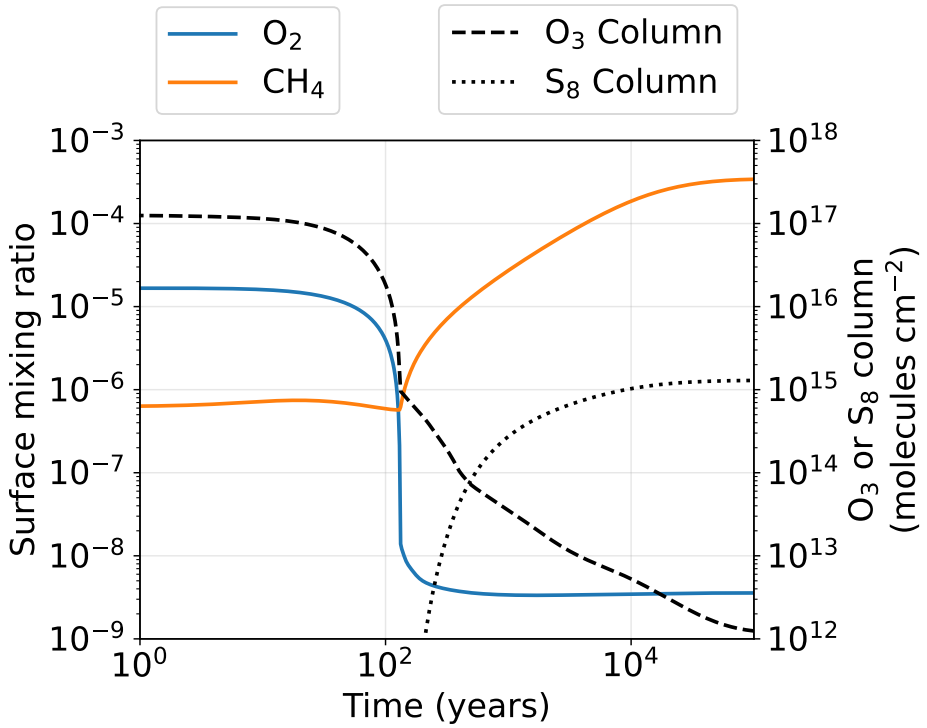

Fig. S4. Modeled oxic to anoxic transition caused by H_2 and CO outgassing from a large igneous province eruption. The simulation begins with a photochemical equilibrium atmosphere, and then is perturbed by a stepwise increase of the H_2 and CO flux by 1.9×10^{11} and 2.0×10^{10} molecules cm^{-2} s^{-1}, respectfully. A LIP eruption should able to produce these outgassing fluxes for the 100 years required to cause O_2 to collapse (see text).

Movie S1. Time dependent photochemical model of the rise of oxygen. This is the same simulation that is shown in Figure 2c in the main text. Left-hand plot shows the mixing ratio of several key species as a function of altitude and time. Right-hand plot shows the photon flux at the top of the atmosphere and the surface as a function of photon wavelength and time. As oxygen rises, and an ozone layer develops, almost all photons < 300 nm are shielded from the surface.

References

1. MW Claire, et al., The evolution of solar flux from 0.1 nm to 160 μm: Quantitative estimates for planetary studies. *The Astrophys. J.* **757**, 95 (2012).
2. N Wogan, J Krissansen-Totton, DC Catling, Abundant atmospheric methane from volcanism on terrestrial planets is unlikely and strengthens the case for methane as a biosignature. *The Planet. Sci. J.* **1**, 58 (2020).
3. S Aulbach, V Stagno, Evidence for a reducing archean ambient mantle and its effects on the carbon cycle. *Geology* **44**, 751–754 (2016).
4. DC Catling, JF Kasting, *Atmospheric evolution on inhabited and lifeless worlds.* (Cambridge University Press), (2017).
5. PJ Wallace, T Plank, M Edmonds, EH Hauri, Volatiles in magmas in *The Encyclopedia of Volcanoes.* (Elsevier), pp. 163–183 (2015).
6. S Self, MF Coffin, MR Rampino, JA Wolff, Large igneous provinces and flood basalt volcanism in *The Encyclopedia of Volcanoes.* (Elsevier), pp. 441–455 (2015).
7. SE Bryan, et al., The largest volcanic eruptions on earth. *Earth-Science Rev.* **102**, 207–229 (2010).
8. N Meyer, A Zerkle, D Fike, Sulphur cycling in a neoarchaean microbial mat. *Geobiology* **15**, 353–365 (2017).
9. E Hairer, G Wanner, *Solving ordinary differential equations II.* (Springer Berlin Heidelberg) Vol. 375, (1996).
10. P Peterson, F2py: a tool for connecting fortran and python programs. *Int. J. Comput. Sci. Eng.* **4**, 296–305 (2009).